China Geology 8 (2025) 500−513

China Geology

Journal homepage: http://chinageology.cgs.cn
https://www.sciencedirect.com/journal/china-geology

Multi-compartmental migration and ecological-health risks of trace metals in Dexing mining concentration areas: A holistic quantitative assessment

Xiao-tao Zhang[a], Jun-jie Hu[b,*], Bin Shen[a], Man-dan Huang[a], Shan-hong Lan[b], Zhi-hang Xin[a]

[a] *National Research Center for Geoanalysis, Chinese Academy of Geological Science, Beijing* 100037, *China*
[b] *School of Environment and Civil Engineering, Dongguan University of Technology, Dongguan* 523808, *China*

ARTICLE INFO

Article history:
Received 13 January 2025
Received in revised form 8 April 2025
Accepted 27 April 2025
Available online 16 July 2025

Keywords:
Copper mining operations
Trace metal(loid)s contamination
Cross-media transfer
Water-amphibians
Soil-earthworms
Air-lichens
DNA methylation biomarkers
Biogeochemical processes
Risk assessment
Sustainable Development Goals (SDG3)
Dexing mining area
Environmental geological survey engineering

ABSTRACT

To address the critical gap in linking multi-compartmental transfer with risks of trace metals (Cd, Pb, As, Cr, Ni) in mining environments. This study systematically investigated the trans-media migration of Cd, Pb, As, Cr, and Ni in China's Dexing copper mining district through paired sampling of water-amphibians, soil-earthworms, and air-lichens. Advanced methodologies were employed, including ICP-MS quantification for heavy metals, geochemical indices (Igeo, BCF, BAF) to assess bioavailability, NMDS for source apportionment, and HPLC to detect DNA methylation alterations. Aquatic systems exhibited severe Cd/Pb enrichment (16.25–24.42 μg/L; 11–15× WHO limits), while agricultural soils showed extreme Cd contamination (1.5 mg/kg; 15× background). Biota displayed metal-specific accumulation: frogs achieved BCFs >1,000 for Pb/Cd, earthworms showed pH-modulated BAFs >2.5 for Cd/As, and lichens recorded 100–1,000× atmospheric Cr enrichment. NMDS resolved three contamination pathways: mining-derived Cd/Pb/As (MDS1 = 2.56), atmospheric Cr (PC2 = 1.84), and geogenic Ni. Cd dominated ecological risks (Eri = 554.25; RI ⩾ 300), while atmospheric Cr drove carcinogenic risks (TCR = 4.11×10^{-5}) exceeding safety thresholds. The source-media-biota-risk framework pioneers the integration of geochemical transport with epigenetic toxicity biomarkers, demonstrating that sub-lethal Cd/Pb exposure induces genome-wide DNA hypomethylation (2.4%–6.6% reduction; $\rho = -0.71$ to -0.91). This paradigm shift prioritizes bioavailability-informed regulations over concentration-based metrics, offering actionable strategies for sustainable development goals-aligned mining pollution control.

1. Introduction

Mining operations represents a critical anthropogenic vector for global trace metal contamination, with cascading impacts on interconnected environmental compartments and ecosystem health (Setu S and Strezov V, 2025). The accelerated extraction and processing of mineral resources disrupt geological metal sequestration mechanisms that have been developed over millennia, liberating persistent pollutants such as cadmium (Cd), lead (Pb), arsenic (As), chromium (Cr), and nickel (Ni) into terrestrial, aquatic, and atmospheric systems (Goodfellow BW et al., 2016). These elements exhibit persistent environmental persistence, bioaccumulative potential, and multi-tiered toxicity, threatening biodiversity, food security, and human health (Edo GI et al., 2024). Contemporary mining practices, particularly in regions with legacy contamination, amplifying these risks through acid mine drainage, particulate emissions, and inadequate waste management, creating complex contamination footprints that exceed single-media assessments (Tran TS et al., 2022). Despite advances in pollution monitoring, critical knowledge gaps persist regarding the cross-media migration mechanisms, bioavailability dynamics, and sub-lethal epigenetic effects of trace metals in mining-impacted ecosystems.

Traditional risk assessment frameworks often prioritize the total metal concentrations while neglecting bioavailability-mediated toxicity and the multi-compartmental transfer pathways (Setu S and Strezov V, 2025). Recent studies have revealed substantial discrepancies between bulk soil metal loads and their ecological impacts, as exemplified by Cd's disproportionate toxicity despite moderate environmental concentrations (Belle GN et al., 2024).

First author: *E-mail address*: zxt347@foxmail.com (Xiao-tao Zhang).

* Corresponding author: *E-mail address*: hujj@edu.dgut.cn (Jun-jie Hu).

Literary editor: Xi-jie Chen
doi:10.31035/cg20250074
2096-5192/© 2025 China Geology Editorial Office.

Furthermore, conventional biomarkers fail to capture chronic exposure effects, such as DNA hypomethylation—a heritable epigenetic modification linked to metal-induced oxidative stress and genomic instability (Hossain MB et al., 2012). The integration of geochemical transport modeling with molecular toxicity endpoints remains underdeveloped, particularly in complex mining landscapes where atmospheric deposition, fluvial transport, and soil-biota interactions synergistically create contamination networks (Liu HL et al., 2021). This disconnect undermines regulatory frameworks aimed at achieving Sustainable Development Goals (SDGs) for clean water (SDG 6), terrestrial conservation (SDG 15), and pollution-related health risk reduction (SDG 3.9).

The Dexing mining region in Jiangxi Province, China—a global epicenter of porphyry copper production—exemplifies these challenges. Intensive mining and smelting activities over decades have generated severe Cd, Pb, and As contamination, with documented metal concentrations exceeding background levels by 15–1000× in soils, aquatic biota, and atmospheric particulates (Ni SQ et al., 2023). Previous studies in this area have focused on single-media contamination or the total metal loads, overlooking the integrated source-media-biota-risk continuum (Wang K et al., 2018). For instance, while Cd-dominated ecological risks in soils have been quantified, the mechanisms driving its exceptional biotransfer to amphibians and earthworms remain poorly understood (Zhu Y et al., 2024). Similarly, atmospheric Cr emissions from ore processing—a potential carcinogen—require evaluation of particulate-phase transport and lichen bioaccumulation patterns (Safe YL et al., 2023). Crucially, no prior work has simultaneously addressed the epigenetic consequences of multi-metal exposure in indicator species, despite evidence linking Cd/Pb to DNA hypomethylation in aquatic and terrestrial organisms (Shafiq S et al., 2019).

This study pioneers a holistic assessment of trace metal dynamics in the Dexing mining ecosystem through paired analysis of water-amphibian, soil-earthworm, and air-lichen systems. This study integrate geochemical indices (Igeo, BCF/BAF), non-metric multidimensional scaling (NMDS), and DNA methylation biomarkers to achieve three objectives: (1) to quantify multi-compartmental contamination levels and spatial heterogeneity; (2) to elucidate metal-specific transfer mechanisms across environmental media; and (3) to evaluate integrated ecological-health risks through novel linkages between bioavailability and epigenetic toxicity. By resolving contamination pathways (e.g., mining-derived Cd/Pb/As versus geogenic Ni), and demonstrating dose-dependent hypomethylation in biota, this work advances predictive models for metal mobility and establishing sub-lethal biomarkers for regulatory frameworks. Our findings provide actionable strategies for source control, bioavailability-informed remediation, and SDG-aligned policy development in global mining regions.

2. Sample selection and analytical technique

2.1. Geological setting

The study area is situated in southeastern China, adjacent to the South China Block (SCB), a geological unit formed through the subduction and amalgamation of the Cathaysia Block with the Yangtze Block during the Neoproterozoic orogeny (Ren Z et al., 2025). The southeastern margin of the SCB hosts the Jiangnan Orogen, a southeast-trending tectonic belt demarcated by the Jiangshan-Shaoxing Fault. This orogen features a complex geological history, including 1.1–0.97 Ga ophiolites, 1.1–0.92 Ga island arc volcanics, about 866 Ma high-pressure blueschists, post-collisional magmatism (870–800 Ma), and foreland basin sedimentation (Ren Z et al., 2025). The SCB's evolution has been profoundly influenced by major tectonic events, such as Triassic collisions with the Indochina and North China Blocks and Early Jurassic northwestward subduction of the Paleo-Pacific Plate beneath the SCB (Zhou Q et al., 2016).

The Dexing Copper Mine, recognized as Asia's largest and China's most ancient open-pit copper deposit, ranks among the world's top ten porphyry copper systems. It contains proven cumulative copper reserves exceeding 9 million tonnes (Mt), contributing approximately 15% of China's total copper production in 2023. When accounting for associated metallic resources, the total metal endowment surpasses 17 Mt. This deposit exemplifies a classic porphyry Cu-Mo-Au system characterized by polymetallic paragenesis, with average grades of 0.45% Cu, 0.01% Mo, and 0.1–0.3 g/t Au. Notably, it hosts critical metals including rhenium, selenium, and tellurium at economically significant concentrations.

2.2. Sampling

Paired soil and earthworm samples were collected from forest ecosystems near the Dexing copper mining district during summer 2022. Sampling coordinates spanned 28°92′57.58″–29°04′90.95″N and 117°52′13.12″–117°69′32.88″E (Fig. 1), covering approximately 720 km^2 of active mining and smelting zones. A total of 22 paired samples were collected. Surface water samples were collected in polytetrafluoroethylene bottles following HJ/T 91-2002 monitoring specifications. Surface soil (0–5 cm depth) was obtained using stainless steel corers. Five subsamples were composited (approximately 100 g) to minimize heterogeneity, stored in labeled polyethylene bags, and preserved at −20°C. Subsets were air-dried, sieved (<63 μm), and homogenized for analysis.

Earthworms (90–110 mm length, reddish-brown morphotype) were collected (200–300 g biomass per site). Specimens were rinsed with deionized water, depurated in ventilated chambers lined with moist filter paper for 24 h, re-rinsed, blotted dry, and weighed. Adult *Rana plancyi* and *R. limnocharis* specimens were collected during their summer activity period from Wuyuan County's national wetland park and a control site near Dexing County. Specimens were visually identified, net-captured, and temporarily stored in

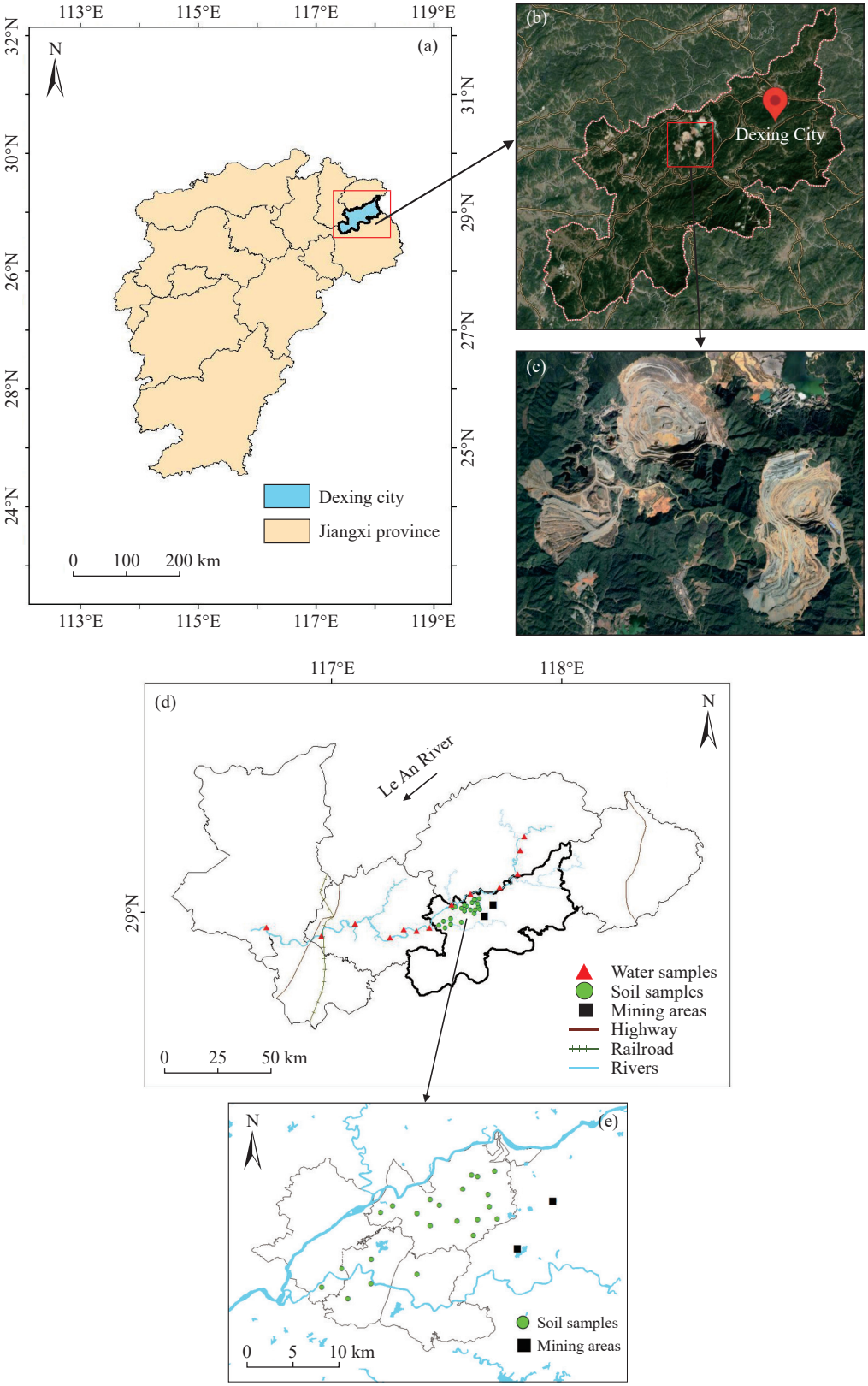

Fig. 1. Map of Dexing mining concentration area, topography and sampling in Dexing City. (a) Location of Dexing City, (b) Location of copper and lead-zinc mines, (c) Topography of copper and lead-zinc mines, (d) River sampling map and (e) Soil sampling map.

native water before laboratory transfer.

2.3. Laboratory analysis

Soil samples (200 mg) underwent microwave-assisted digestion ($HClO_4$-HNO_3-HF-H_2O_2) in polytetrafluoroethylene vessels following China's Soil Environmental Quality Standard (GB 15618-2018). Water samples were 0.45-μm glass fiber-filtered and acidified to pH = 2 with ultrapure HNO_3. Digested solutions were filtered, evaporated to near-

dryness, and reconstituted. Batch analyses included six replicates along with blanks and certified reference material (GBW07428). Trace metal concentrations (Cd, Pb, As, Cr, Ni) were quantified via inductively coupled plasma mass spectrometry (ICP-MS; Agilent 7500ce; detection limit: 0.01 μg/mL). Method accuracy was validated through GBW07428 recovery rates (recoveries 95%–105%) and relative standard deviations (<10%).

Earthworm and frog (50 mg) tissue were digested in HNO_3/H_2O_2 (1∶1 v/v), diluted to 25 mL, and analyzed via inductively coupled plasma-mass spectrometry (ICP-MS) using GBW07603 reference material (recoveries 89%–97%). Lichens were rinsed with distilled water, oven-dried (60 °C, >48 h), crushed using an agate mortar, and sieved (<2 mm) after impurity removal. Water and liver trace metal data were validated against certified reference material GBW07603, with quality assurance via triplicate analyses. Method accuracy was confirmed through certified reference material for shrub branches/leaves recoveries (89%–97%, n=6).

2.4. Assessment metrics

Integrated assessment of trace metal distribution, migration, and transformation in mining areas was conducted using multiple indices: geoaccumulation index (Igeo), single factor pollution index (CF), trace metal evaluation index (HEI), potential ecological risk index (Eri), and NMDS analysis. Bioavailability and toxicity were evaluated using bioconcentration factor (BCF), bioaccumulation factor (BAF). Health risks from atmospheric particulates were assessed via CalTOX modeling with hazard index (HI) and total carcinogenic risk (TCR). All calculations utilized measured trace metal concentrations across the media compartments. Detail information is provided in Supplementary Materials.

2.5. Health risk assessment

Human health risks were assessed by quantifying average daily exposure (ADE) through ingestion (ADE_{ing}), dermal contact (ADE_{der}), and inhalation (ADE_{inh}) pathways (mg/kg/day) using California EPA's CalTOX geochemical model (Matlock M et al., 2005).

$$ADE_{ing} = C_i \times \frac{IR_{ing}}{BW} \times FI \times \frac{EF \times ED}{AT} \times 10^{-6} \quad (1)$$

$$ADE_{der} = C_i \times \frac{AF \times ABS \times SA}{BW} \times FC \times \frac{EF \times ED}{AT} \times 10^{-6} \quad (2)$$

$$ADE_{inh} = C_i \times \left\{ (ET \times f_i \times BR_l) + \left[ET \times (1 - f_i) \times BR_h \right] \right\} \times \frac{EF \times ED}{AT \times PEF} \quad (3)$$

Health risk assessment parameters were defined as follows:: C_i (metal concentration in air, mg/kg), ED (exposure duration, years), BW (body weight, kg), AT (averaging time, days), IR (ingestion rate, mg/day), AF (dermal adhesion coefficient, mg/cm^2), ABS (dermal absorption factor), EF (exposure frequency, days/year), SA (exposed skin area, cm^2), FI (fraction of ingested particulates from contaminated areas), FC (fraction of dermal-adhered particulates from contaminated areas), ET (daily inhalation duration in target zone, hours/day), BR_l (light-activity breathing fraction, m^3/kg/hour, 80% of inhalation duration), BR_h (heavy-activity breathing fraction, m^3/kg/hour).

Non-carcinogenic risk was quantified for three pathways:

$$HQ_j^i = \frac{ADE_j^i}{RfD_j^i} \quad (4)$$

$$HI = \sum_{i=1}^{m} \sum_{j=1}^{n} HQ_j^i \quad (5)$$

Non-carcinogenic risks were assessed via hazard quotient (HQ) for metal i through pathway j (ingestion, dermal contact, inhalation), with the Hazard Index (HI) representing cumulative HQ across all metals. Risks were considered negligible if HQ or HI <1 (USEPA, 2001). RfD_j^i denotes the reference dose (mg/kg/d) for trace metals.

Carcinogenic risk (CR) was calculated as follows:

$$CR_j^i = ADE_j^i \times CSF_j^i \quad (6)$$

$$TCR = \sum_{i=1}^{m} \sum_{j=1}^{n} CR_j^i \quad (7)$$

CR_j^i is the cancer risk for metal i through pathway j (ingestion, dermal contact, inhalation). CSF_j^i is the cancer slope factor for trace metal (mg/kg/day). TCR (total carcinogenic risk) thresholds were defined as: $<10^{-6}$ (negligible), 10^{-6}–10^{-4} (acceptable), $>10^{-4}$ (unacceptable) (Howlader M et al., 2025).

2.6. DNA methylation analysis

Earthworm and frog genomic DNA was extracted using TIANGEN kits (China). DNA methylation levels were determined following procedures published in our previous study (Hu JJ et al., 2021). Detail information were provided in Supplementary Materials.

2.7. Statistical analysis

Normality was assessed using Kolmogorov-Smirnov and Shapiro-Wilk tests. Spatial differences were analyzed using Kruskal-Wallis and Wilcoxon tests. Spearman correlations (p<0.05) were used to determine relationships between metals across media compartments. Graphics were generated using Cloudtutu, ArcMap 10.2, and Adobe Illustrator tools. Analyses were performed using SPSS 25.

3. Results and discussion

3.1. Geochemical characteristics of trace metals

3.1.1. Trace metal concentrations

Environmental compartments exhibited distinct trace

metal contamination profiles (Table 1). River water systems displayed severe anthropogenic enrichment, with mean concentrations (μg/L) descending as As (24.42) > Pb (16.25) > Ni (14.33) > Cd (6.73) > Cr (4.67), representing 1.17–21.50-fold elevations relative to upstream reference sites. Critically, Pb and cadmium exceeded China's Grade I/II surface water standards (GB 3838-2002) (Table S1), while Pb, Cd, and As collectively surpassed WHO drinking water guidelines (World Health Organization, 2017) and EU regulatory thresholds (Ersoz M and Barrott L, 2012). Agricultural soils demonstrated extreme Cd contamination (median: 1.5 mg/kg; 15.0× Jiangxi background) and significant As enrichment (45.3 mg/kg; 4.4× background), violating China's Soil Quality Guidelines (GB 15618-1995/2018) (Table S2), Canadian (CCME) (Robaldi-Vázquez MP et al., 2025), Dutch (Swartjes FA, 1999), and Iranian (Faraji M et al., 2023) regulatory limits. Pb (58.4 mg/kg; 1.8× background) further contributed to soil pollution, whereas Cr and Ni approximated geogenic levels. Atmospheric deposition fluxes were dominated by Pb accumulation (0.91 mg/cm^2 leaf surface), exceeding Cd (0.004 mg/cm^2) and Cr (0.06 mg/cm^2) by orders of magnitude, consistent with long-range transport from mining/smelting emissions within a 2.88-km radius (Liu HL et al., 2021; Safe YL et al., 2023).

Biota accumulated metals at hazardous levels across trophic levels. Hepatic concentrations in amphibians (*Rana plancyi* and *R. limnocharis*) reached 15.36–17.37 mg/kg for Pb and 5.77–6.13 mg/kg for Cd, exceeding WHO safety thresholds (1.00 mg/kg Pb; 0.50 mg/kg Cd) by >15-fold and >11-fold, respectively (Table 2 and S3), with 5.71× enrichment relative to control specimens (Ediagbonya TF et al., 2022). Earthworm tissues contained elevated Pb (43.07–346.01 mg/kg), Cd (2.29–5.63 mg/kg), and As (39.31–93.43 mg/kg), surpassing reference ecosystem baselines (Ediagbonya TF et al., 2022). Lichens proximal to mining operations accumulated Pb (265.75 mg/kg), Cd (1.99 mg/kg), and Cr (52.07 mg/kg) (Table S4), at 100–1,000× baseline levels documented in Portuguese (IAEA-336) (Heller-Zeisler S et al., 1999) and Canadian studies (Singh SM et al., 2013), corroborating particulate deposition from copper smelters. This contamination signature aligns with Dexing's mantle-derived copper deposit (Ren Z et al., 2025), evidenced by pyrite Pb-isotope ratios matching host porphyries, resulting in soil and vegetation metal loads exceeding global mining benchmarks.

3.1.2. Spatial distribution of trace metals across sampling sites

Trace metal concentrations exhibited significant spatial heterogeneity across sampling sites, driven primarily by mining activities. In aqueous samples, Cd and Pb displayed extreme deviations from normal distributions, characterized by strong positive skewness (1.19–2.73) and high kurtosis (Cd: 7.94; Pb: 5.89), indicating localized contamination hotspots downstream of mining operations (Table 1). In contrast, As showed a multimodal dispersion pattern with negative skewness (−0.66) and platykurtic kurtosis (0.23), suggesting complex transport pathways. Atmospheric deposition exhibited near-normal distributions (skewness: −0.66–0.40; kurtosis: −0.71–0.04), reflecting homogeneous particulate dispersion from smelting emissions. Notably, aqueous Pb demonstrated conflicting normality results (Kolmogorov-Smirnov $p > 0.05$ vs. Shapiro-Wilk $p < 0.05$), resolved graphically as a mild left-skewed distribution.

Spatial variability, quantified by coefficients of variation (CV), further highlighted compartment-specific patterns:

Table 1. Concentrations of trace metals in river, soil and atmospheric deposition.

Medium	Sampling	Pb	Cd	As	Cr	Ni
River (ng/mL)	Mining	3.04–41.05(14)	0.44–43.14(1)	14.22–32.33(26)	2.05–9.21(4)	2.05–58.03(8)
	Control	16.23	2.44	18.18	5.02	17.13
	Skewness	2.12	2.73	-0.66	1.19	1.70
	Kurtosis	5.89	7.94	0.23	1.16	1.60
Soil (mg/kg)	Mining	34.30–429.19(58.35)	0.50–7.94(1.50)	33.65–113.45(45.29)	42.11–147.06(64.08)	13.88–60.47(31.28)
	Skewness	3.31	2.52	1.80	1.96	0.63
	Kurtosis	12.73	6.49	2.79	5.38	-0.34
Air (mg/cm^2)	Mining	0.73–1.13(0.89)	0.000–0.009(0.0035)	ND	0.04–0.07(0.06)	ND
	Skewness	0.40	0.36	ND	-0.66	ND
	Kurtosis	0.04	-0.63	ND	-0.71	ND

ND: not detected

Table 2. Concentration of trace metals in frogs (*Rana plancyi* and *Rana limnocharis*), earthworm and lichen (mg/kg).

HMs	*Rana plancyi*		*Rana limnocharis*		Earthworm	Lichen
	Mining	Control	Mining	Control		
Pb	14.21–20.16 (17.82)	2.54–4.23 (3.12)	11.73–16.60 (15.89)	3.65–5.65(4.12)	43.07–346.01(157.27)	105.70–1066.00(265.75)
Cd	4.72–7.62 (5.98)	1.96–2.51 (2.13)	4.84–6.65 (6.00)	2.99–3.85(3.14)	2.29–5.63(3.82)	1.49–2.98(1.99)
As	0.07–0.24 (0.16)	0.01–0.04 (0.03)	0.16–0.22 (0.19)	0.03–0.07(0.05)	39.31–93.43(48.66)	ND
Cr	0.81–1.34 (0.97)	0.19–0.44 (0.26)	0.81–1.34 (0.93)	0.22–0.35(0.28)	38.97–86.52(68.35)	15.97–72.68(52.07)
Ni	3.54–5.52 (4.74)	1.92–3.56 (3.11)	3.38–4.86 (3.97)	2.43–4.32(3.43)	16.43–52.58(32.34)	ND

ND: not detected

aqueous Cd (CV = 1.75) and Pb (CV = 1.13) exceeded thresholds for strong variability (CV ⩾ 1), while soils showed moderate heterogeneity (Pb CV = 0.92; Cd CV = 0.76). Atmospheric metals displayed low variability (Cd CV = 0.63; others < 0.5), consistent with uniform emissions. Critically, strong spearman correlations between Pb and Cd in water (ρ = 0.68, $p < 0.01$) and soil (ρ = 0.65, $p < 0.01$) confirmed shared anthropogenic sourcing and geochemical behavior. These integrated spatial signatures identify mining as the dominant driver of trace metal heterogeneity, with Cd and Pb governing multi-media pollution gradients.

3.1.3. Geochemical indices of trace metals

Riverine contamination patterns revealed Cd and Pb as the primary pollutants through single factor pollution index (CF) analysis. Cd exhibited severe contamination (mean CF = 6.73), while Pb showed moderate pollution (CF = 1.63). In contrast, As (CF = 0.49), Cr (CF = 0.47), and Ni (CF = 0.72) remained below contamination thresholds (Table 3). Peak pollution localized downstream aligns with sediment contamination patterns observed in mining-impacted rivers globally, such as Colombia's San Jorge River (Marrugo-Negrete J et al., 2021), where Cd, Pb, and As enrichment induced moderate-to-severe ecological risks. Although the mean trace metal evaluation index (HEI) indicated overall low contamination (<10), two downstream stations exceeded moderate/severe thresholds due to concentrated Pb, Cd, and As enrichment—a phenomenon documented across mining-affected fluvial systems in China, Romania, and Ecuador (Bai HL et al., 2024; Moldovan A et al., 2022; Park S and Kim Y, 2016). This underscores the ecotoxicological imperative for targeted mitigation of Cd and Pb in aquatic compartments.

Soil geoaccumulation indices (Igeo) demonstrated pronounced anthropogenic dominance of Cd (median Igeo = 3.66; range: 2.08–6.07), classifying soils as moderately to strongly contaminated (Table 3). As ranked second (median Igeo = 1.54; range: 1.11–2.86), indicating moderate contamination, while Pb (Igeo = 0.28), Ni (Igeo = 0.13), and Cr (Igeo = −0.17) showed negligible-to-uncontaminated status. This Cd enrichment profile mirrors global mining regions, where industrial emissions, tailings weathering, and acid drainage collectively elevate soil Cd burdens (Cai K and Li C, 2022; Zhu Y et al., 2024), as evidenced in China's coastal zones, Niger Delta, and Southwest Asia (Chris DI et al., 2023; Jahandari A and Abbasnejad B, 2024; Pal D et al., 2022). Atmospheric deposition exhibited Pb flux dominance (0.73–1.13 mg/cm^2 leaf surface), implicating mining/smelting emissions as principal contributors—consistent with patterns near industrial zones in China (Chen YZ et al., 2022), Jordan (Chien C et al., 2019), and the U.S. (Laidlaw MAS et al., 2023). Significant Pb-Cr correlation (ρ = 0.718, $p < 0.01$) suggested shared transport pathways (e.g., fugitive dust from ore transport), though regional heterogeneity exists, as noted in Southwest Iran (Moaref S et al., 2014). Notably, Cinnamomum camphora foliage preferentially accumulated atmospheric Pb/Cd over bark substrates, highlighting species-specific biomonitoring utility in mining landscapes.

Table 3. Contents of single factor pollution index (CF) and geoaccumulation index (Igeo) in river and soil.

HMs	River	Soil
	CF	Igeo
Pb	0.20–5.80 (0.80)	−0.49–3.16 (0.28)
Cd	0.40–43.00 (0.95)	2.08–6.07 (3.66)
As	0.28–0.64 (0.52)	1.11–2.86 (1.54)
Cr	0.20–0.90 (0.40)	−0.77–1.03 (-0.17)
Ni	0.15–2.05 (0.68)	−1.04–1.09 (0.13)

3.2. Multi-compartmental partitioning of trace metals

3.2.1. Multi-compartmental transfer characterization

Amphibians function as critical bioindicators of trace metal mobility due to their intermediate trophic position and environmental sensitivity (Tatlı H et al., 2024), with bioconcentration factors (BCF) revealing pronounced species-specific transfer efficiencies where *Rana plancyi* exhibited Pb and Cd BCFs of 1096.62 and 889.22 respectively, while *Rana limnocharis* showed 977.85 (Pb) and 892.19 (Cd)—both approaching the high-bioaccumulation threshold (>1000) and confirming the hierarchy Pb > Cd > Ni > Cr > As (Table 4). This reflects preferential dissolved-phase metal uptake, though ligand complexation may reduce bioavailability, while significant correlations ($p < 0.05$) linked aqueous Pb/As/Cr/Ni to R. plancyi tissues and As/Cr/Ni to *R. limnocharis* (Tariq A and Farhat F, 2025). The absence of water-tissue Pb/Cd correlations in *R. limnocharis* indicates non-conservative transfer mediated by dietary exposure and dynamic riverine fluxes, where hydrochemical parameters (flow velocity, pH, Eh, salinity) critically modulate speciation (Chi WT et al., 2022)—high-flow regimes dilute aqueous Cd whereas riparian habitat preferences enhance sediment-bound metal exposure (Kumari M and Bhattacharya T, 2023), evidenced by 25.48× Cd and 4.63× Pb enrichment downstream with confirmed spatial differentiation (Kruskal-Wallis, Cd: $p < 0.05$) (Table S5). These patterns align with Pb-Zn mining districts where surface/groundwater transport metals to adjacent ecosystems, though biogeochemical barriers may mitigate mobility (Chen XH et al., 2025); concurrently, trophic transfer via aquatic insects and bivalves amplifies

Table 4. Contents of bioconcentration factor (BCF) in frogs (*Rana plancyi* and *Rana limnocharis*) and bioaccumulation factor (BAF) in earthworm.

HMs	*Rana plancyi*	*Rana limnocharis*	Earthworm
	BCF	BCF	BAF
Pb	874.46–1240.62 (1096.62)	721.85–1021.54 (977.85)	0.74–5.93 (2.70)
Cd	701.86–1133.09 (889.22)	719.70–988.85 (892.19)	1.52–3.76 (2.54)
As	2.87–9.83 (6.55)	6.55–9.01 (7.78)	0.87–2.06 (1.07)
Cr	173.57–287.14 (207.86)	173.57–287.14 (199.29)	0.61–1.35 (1.07)
Ni	246.98–385.12 (330.70)	235.81–339.07 (276.98)	0.53–1.68 (1.03)

hepatic retention due to limited detoxification (Tabassum S et al., 2024), and while As/Cr/Ni show lower transfer efficiencies, their biogeochemical persistence remains concerning. Chronic Cd/Pb exposure disrupts oxidative balance and epigenetic regulation (Köse E, 2024; Singh D et al., 2025), necessitating mechanistic studies on enzymatic/gene dysregulation, and collectively demanding integrated frameworks to monitor multi-compartmental dynamics in mining landscapes.

The bioaccumulation factor (BAF) quantifies trace metal transfer from soil to biota (Wang K et al., 2018). Earthworms exhibited preferential accumulation of Pb (BAF: 2.70) and Cd (BAF: 2.54), exceeding As, Cr, and Ni (BAF >1) (Table 4), with Cd showing enhanced mobility through higher variability (2.749 ± 0.441). Significant soil-earthworm Cd correlation (ρ=0.56, p<0.05) corroborated Pb/Cd co-accumulation patterns (Table S6 and S7), attributed to soil matrix interactions and co-mobilization effects (Liu HL et al., 2024). Bioavailability was modulated by chemical speciation and edaphic factors (pH, Eh, organic matter), particularly in acidic mining soils where pH gradients disproportionately enhanced Cd transfer (Gantayat RR and Elumalai V, 2024). Metal-induced biomass suppression reflected these dynamics, while intraspecific physiological variations contributed to BAF heterogeneity. Mining activities drove agricultural soil enrichment, enabling trophic transfer of Pb/Cd/As even in organically amended soils, causing chronic growth inhibition and genotoxicity (Zhu Y et al., 2024). Critically, co-contaminants (microplastics, pesticides) amplified metal bioavailability through synergistic interactions, facilitating cross-kingdom food web transfer (Gruss I et al., 2024). Legacy contamination persisted decades post-mining, evidenced by rehabilitated Slovakian soils exceeding risk thresholds 18 years after remediation (Demková L et al., 2017), underscoring enduring agroecosystem threats and global biogeochemical cycle disruptions.

Lichens serve as sensitive bioindicators of airborne metal fluxes due to their direct nutrient acquisition from the atmosphere (Garty J, 2001), with significant positive correlations confirming atmospheric deposition as the primary Cd source (ρ = 0.31, p < 0.05) (Table 5 and S7). This aligns with global patterns: transplanted lichens in western Greenland's Pb-Zn mining area showed 1.4–5× Pb/Cd enrichment after one-year exposure (Søndergaard J et al., 2013), while European-scale moss monitoring demonstrated significant atmosphere-Pb/Cd correlations in >66% of surveyed nations (Harmens H et al., 2012). Mining activities drive metal mobilization through wind/rain erosion of waste piles—exemplified at Balya's abandoned mine where open-air deposits elevated surrounding lichen burdens —with Dexing's copper complex identified as a major emission hotspot (Santos NL et al., 2022). Persistent atmospheric dispersion explains anomalous Pb accumulation in lichens, facilitating long-range transport evidenced by Pb/Cd/As enrichment in China's remote mountains and arctic regions (Bing HJ et al., 2019; Rudnicka-Kępa P et al., 2024). Metal-laden particulates impair lichen physiology, inducing species-specific responses: tolerant taxa (e.g., *Xanthoria* parietina) proliferate while sensitive species (e.g., Evernia prunastri) decline (Paoli L et al., 2011). These biogeochemical shifts underscore complex atmosphere-biosphere interactions with cascading ecosystem impacts, necessitating integrated frameworks to mitigate cross-media contamination risks in mining zones.

Table 5. Correlation coefficients of trace metal concentrations between atmosphere and lichen.

	Pb	Cd	Cr
Atmosphere-lichen	0.29	0.31*	0.24

* p<0.05, ** p<0.01 (two−tailed)

3.2.2. Integrated analysis of multi-compartmental biotransfer

The geochemical behavior of trace metals across interconnected environmental compartments revealed distinct partitioning patterns governed by source dynamics and biogeochemical processes (Fig. 2). Cr and Ni exhibited limited mobility in aquatic-terrestrial systems, with low bioconcentration factors (BCF < 50 in frogs; BAF < 1 in earthworms), aligning with their predominantly lithogenic origins and strong affinity for soil mineral matrices (Adhikari S et al., 2022). Lichen Cr concentrations, however, exceeded background levels by 50×, implicating atmospheric deposition —rather than soil-mediated transport —as the dominant pathway, consistent with global studies attributing Cr enrichment to direct dust/gaseous emissions from mining/smelting. As demonstrated moderate persistence in soils (Igeo=1.54) but showed selective bioavailability, with earthworm BAF values (1.32 ± 0.24) reflecting its partial mobilization under acidic conditions (pH = 5.2–6.8) prevalent in mining-affected soils and also highlighting soil-specific ecotoxicological risks. In contrast, Cd and Pb dominated cross-media transfer, achieving maximum BCF values of 1096.62 (Pb in *Rana plancyi*) and 892.19 (Cd in *Rana limnocharis*), surpassing thresholds for high bioaccumulation (>1000) (GB/T 31270.7–2014). This exceptional mobility stemmed from Cd's preferential adsorption onto dissolved organic matter (DOM) and Pb's association with fine particulate colloids (<0.45 μm), enhancing their bioavailability in aqueous systems. Cd's exceptional mobility across pH gradients facilitated cross-compartmental transport, linking aqueous, atmospheric, and soil reservoirs. Notably, Pb exhibited moderate soil contamination (median Igeo = 0.28) but high soil-to-earthworm transfer efficiency (BAF=2.70), underscoring bioavailability decoupled from bulk soil concentrations. Spatial heterogeneity further amplified risks: downstream Cd concentrations in frog livers reached 6.13 mg/kg (12×WHO limits), while Pb accumulation in lichens (265.75 mg/kg) mirrored deposition patterns within the range of smelting zones (Liu HL et al., 2021). Such dynamics underscore the decoupling between total metal concentrations and ecological impacts—Cd's extreme ecological risk (Eri = 554.25) despite moderate soil loads (1.5 mg/kg) highlights bioavailability as the critical risk determinant (Setu S and Strezov V, 2025).

NMDS (stress = 0.0064) resolved contamination pathways, showing strong clustering of Cd, Pb, and As across

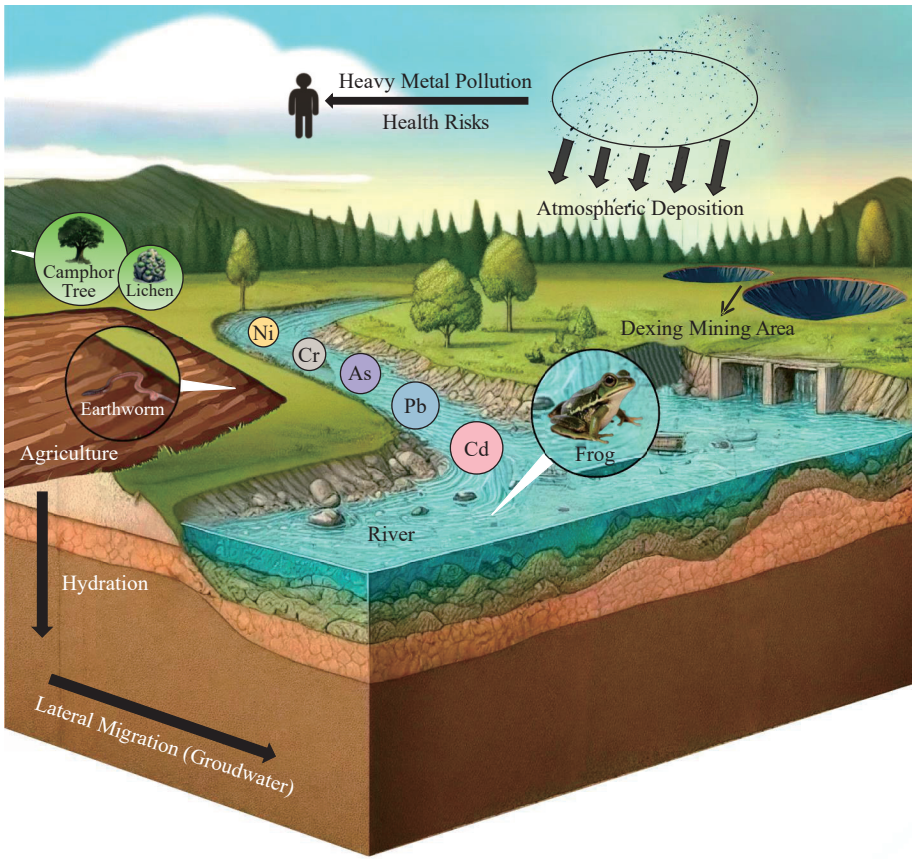

Fig. 2. Geochemical map of trace metal transfer across surface media (The base map of this figure was generated by ChatGPT with the prompt: "Create a diagram illustrating the trace metal transfer across surface media", and verified by the authors.).

water-soil-air matrices (MDS1: 0.62–2.56), confirming their shared anthropogenic origin (Fig. 3). Ni consistently clustered with background values, confirming its geogenic derivation from bedrock weathering (Gasparatos D and Barbayiannis N, 2018). Atmospheric Pb-Cr correlations (ρ = 0.718) implicated fugitive dust from ore transport and tailings weathering as key vectors (Safe YL et al., 2023), while Ni's alignment with geogenic baselines reflected bedrock weathering inputs (Gasparatos D and Barbayiannis N, 2018). Notably, Pb's low soil contamination (Igeo = 0.28) contrasted with its high earthworm BAF (2.70), emphasizing the inadequacy of bulk soil metrics for risk assessment. This discrepancy parallels findings in Pb-Zn mining regions, where sub-micron particulates bypass soil retention mechanisms to directly contaminate biota (Simatupang CA et al., 2025). Technophility indices prioritized Cd (140) >> Pb (30) > Cr (4), consistent with Cd's capacity to disrupt epigenetic regulation (DNA hypomethylation: ρ = −0.71 in frogs) (Table S9) even at sub-lethal concentrations (Hossain MB et al., 2012). The multi-compartment framework thus identifies Cd/Pb as keystone pollutants requiring source containment (e.g., tailings encapsulation, phytostabilization), while Cr demands emission controls targeting airborne particulates. These findings collectively demonstrate that trace metal mobility and ecotoxicological risk are governed not solely by total environmental concentrations, but by dynamic interactions among metal speciation (e.g., Cd solubility across pH gradients), biogeochemical conditions, and biotic uptake

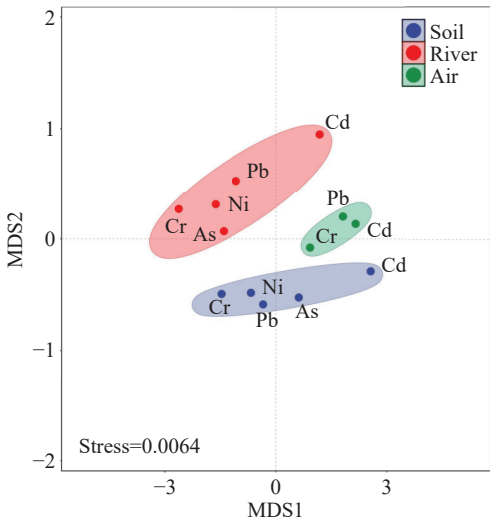

Fig. 3. Distribution pattern of trace metals in soil-river-air system from the Dexing copper mining area characterized by non-metric multidimensional scaling (NMDS).

pathways, establishing Cd and Pb as priority contaminants requiring targeted mitigation in mining landscapes.

3.3. Environmental health risk assessment

Ecological risk index (Eri) values of metals in water and soils were provided in Table 6. Cd emerged as the paramount ecological threat in river systems, exhibiting high-to-extreme

risk downstream (Eri = 554.25) despite generally low metal loads, while other metals posed minimal hazards (Eri < 40). This Cd dominance, consistent with contamination factor trends, contributed >80% of comprehensive ecological risk (RI ≥ 150) - a pattern aligning with uranium mining-impacted watersheds globally (Zheng LL et al., 2020). Paradoxically, Pb demonstrated negligible aquatic risk due to its low toxicity coefficient, yet exhibited exceptional bioconcentration in frogs (BCF > 1000), suggesting either habitat-specific bioavailability or uncharacterized trophic transfer mechanisms requiring toxicological interrogation.

Agricultural soils manifested parallel Cd-centric hazards, with ecological risk indices descending: Cd (Eri = 450.00) >> As (43.54) > Pb/Ni/Cr (<10) (Table 6). Despite moderate absolute concentrations, Cd imposed extreme ecological risk universally (Eri ≥ 320), while Cr's substantial soil burdens translated to minimal hazard. The comprehensive risk index (RI ≥ 300) confirmed considerable-to-extreme threats across all sites, with Cd and As accounting for 87.50% and 8.45% of total risk respectively (Fig. 4 and 5). This profound disconnect between Cd's environmental persistence and outsized ecotoxicity underscores bioavailability - rather than total concentration - as the critical risk determinant, consistent with global mining-impacted regions (Setu S and Strezov V, 2025).

Non-carcinogenic hazard indices (HQ) for atmospheric Pb, Cd, and Cr via ingestion, dermal contact, and inhalation pathways were <1 (Table 7), with total hazard index (HI) of 0.12 (adults) and 0.05 (children). Total carcinogenic risks (TCR) fell within acceptable ranges (adults: 4.11×10^{-5}; children: 1.73×10^{-5}) (Table S10-S12), though exceeding the 10^{-5} threshold, primarily driven by Cr and Cd. The CalTOX model's conservative parameterization likely underestimates risks compared to RBCA and CLEA frameworks (Jia XY et al., 2012). Contrary to typical exposure paradigms, adults exhibited higher risks than children in this study—a pattern corroborated by Matlock M et al. (2005) using CalTOX. Technophility indices prioritized Cd (140) >> Pb (30) > Cr (4), aligning with Cd's exceptional biogeochemical mobility (Bashkin VN, 2007) and epidemiological evidence linking chronic Cd/Cr exposure to pulmonary/gastric/renal pathologies in mining communities across China, Ghana, and Southeast Asia. Critically, acid deposition amplifies these threats by enhancing Cd mobilization through food webs, necessitating integrated source controls targeting metallurgical residues and atmospheric emissions to disrupt exposure pathways.

Table 6. Contents of ecological risk index (Eri) in river and soil.

HMs	River	Soil
Pb	1.00–29.00 (4.00)	5.34–66.85 (9.09)
Cd	12.00–1290.00 (28.50)	150.00–2380.95 (450.00)
As	2.80–6.40 (5.20)	32.36–109.08 (43.54)
Cr	0.40–1.80 (0.80)	1.75–6.13 (2.67)
Ni	0.75–10.25 (3.38)	3.65–15.91 (8.23)

3.4. Environmental adverse effects

Trace metal exposure perturbs epigenetic regulatory networks across diverse taxa, with cascading ecological consequences. In earthworms (*Lumbricus rubellus*), genomic DNA methylation levels (2.40%–6.60%) showed significant inverse correlations with soil Cd (Cd: $\rho = -0.56$, $p < 0.05$) (Table S13) and As concentrations, aligning with chronic exposure-induced hypomethylation patterns observed in prior studies. This absence of direct genome-wide methylation-metal correlations likely reflects temporal decoupling: metal bioaccumulation integrates long-term biogeochemical cycling, whereas epigenetic marks capture transient physiological responses. Elevated Cd/Pb bioavailability (BCF > 1,000) suggests persistent environmental stressors drive this

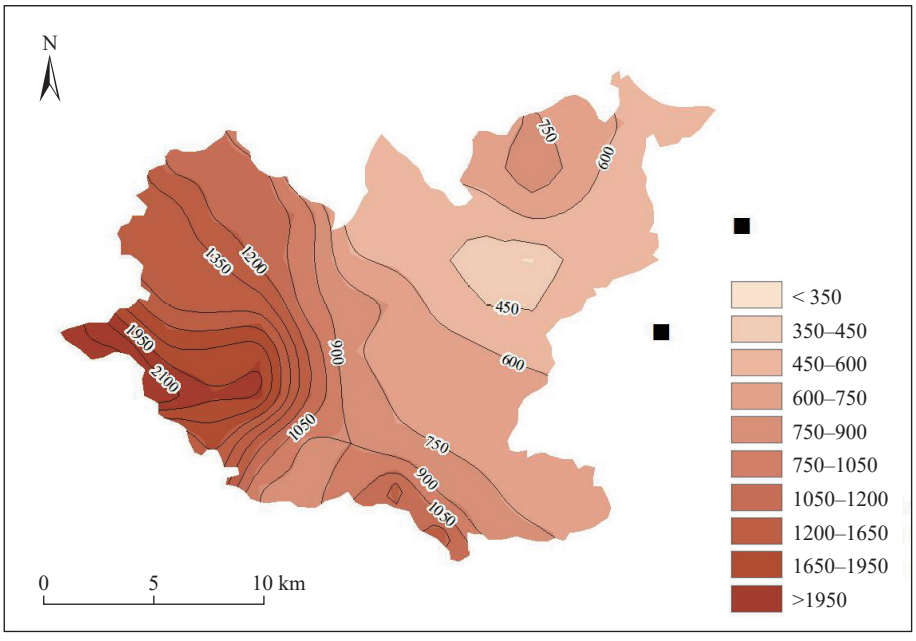

Fig. 4. Biogeochemical mapping of ecological risk index (RI) for trace metal in Dexing mining concentration area.

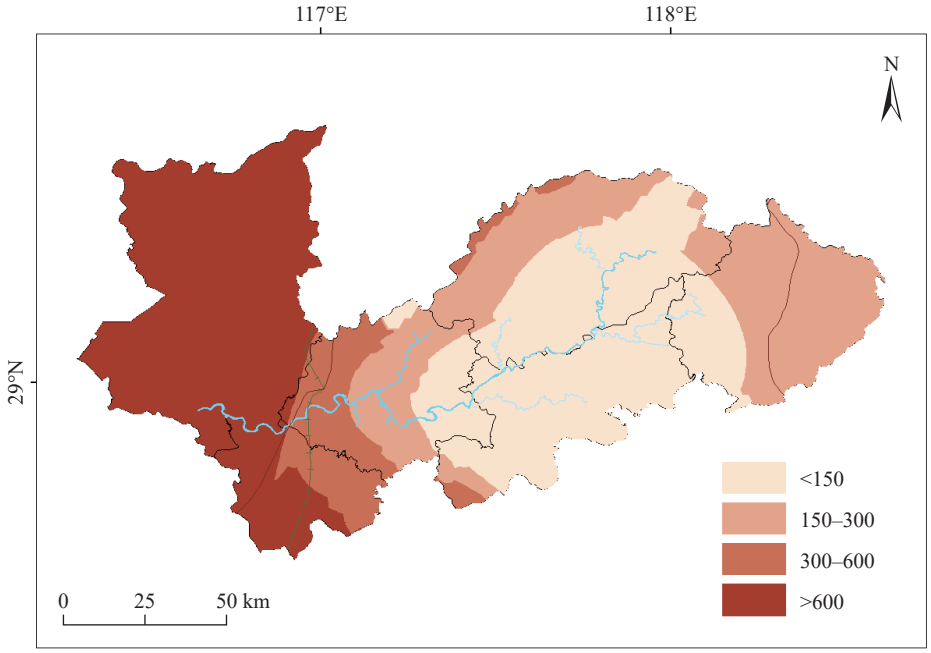

Fig. 5. Ecological risk index (RI) map of trace metal in water.

Table 7. Non-carcinogenic hazard indices (HQ), total hazard index (HI), carcinogenic risk (CR) and total carcinogenic risk (TCR) of adults and children.

HMs	Adults			HI	Children			HI
	HQ_{ing}	HQ_{der}	HQ_{inh}		HQ_{ing}	HQ_{der}	HQ_{inh}	
Pb	9.62E-02	7.08E-04	2.21E-06	0.12	3.87E-02	7.47E-04	1.13E-06	0.05
Cd	1.99E-03	2.18E-04	1.53E-08		8.02E-04	2.30E-04	7.86E-09	
Cr	1.66E-02	9.10E-04	4.03E-07		6.69E-03	9.60E-04	2.06E-07	
	CR_{ing}	CR_{der}	CR_{inh}	TCR	CR_{ing}	CR_{der}	CR_{inh}	TCR
Pb	2.86E-06	–	3.26E-10	4.11E-05	1.15E-06	–	1.67E-10	1.73E-05
Cd	1.22E-05	1.33E-08	2.90E-10		4.89E-06	1.40E-08	1.49E-10	
Cr	2.50E-05	1.09E-06	4.84E-08		1.00E-05	1.15E-06	2.48E-08	

hypomethylation —a finding contrasting with Cd-induced hypermethylation documented in model organisms like Arabidopsis thaliana and rat hepatocytes, where compensatory gene regulation mechanisms prevail.

In amphibians inhabiting mining-affected streams, hepatic DNA hypomethylation was pronounced in exposed *Rana plancyi* (0.44%–5.97% vs. controls; p<0.05) and *Rana limnocharis* (2.10%–4.49%) (Table S13). Notably, species-specific susceptibility emerged: R. plancyi exhibited strong negative correlations with Cd ($\rho = -0.71$, $p < 0.01$) and As ($\rho = -0.54$, $p < 0.05$), while *R. limnocharis* showed dominant associations with Pb ($\rho = -0.72$, $p < 0.01$) and As ($\rho = -0.91$, $p < 0.01$) (Fig. 6). These differential responses align with exceptional Pb/Cd bioaccumulation (BCF > 1,000) and extended amphibian lifespans, which amplify cumulative epigenetic dysregulation compared to shorter-lived invertebrates (Galati S et al., 2021). Mechanistically, metals disrupt epigenetic homeostasis through enzyme inhibition (e.g., As downregulating DNMTs and depleting methyl donors like SAM) (Nohara K et al., 2011), signaling interference (Cd dysregulating Ca^{2+}/CaMKII pathways to activate MAPK-dependent epigenetic modifiers) (Wu XH et al., 2020), chromatin remodeling (metal-induced HDAC/HAT inhibition altering histone methylation/acetylation) (Shafiq S et al., 2020), and oxidative cascades (ROS causing DNA strand breaks that divert repair resources from methylation maintenance) (Jing MY et al., 2022).

Field evidence from India's contaminated wetlands corroborates these processes, with Euphlyctis hexadactylusexhibiting immunosuppression and developmental defects stemming from similar epigenetic disruption (Priyadarshani S et al., 2015). Collectively, mining activities initiate biogeochemical cascades —metal mobilization through trophic transfer induces epigenetic dysregulation that compromises genomic stability (Mao SX et al., 2024). These alterations represent persistent environmental footprints that diminish population resilience long after initial contaminant exposure, revealing a critical pathway by which Cd, Pb, and As undermine ecosystem health even following source remediation.

4. Conclusions

(i) Mining activities induced severe trace metal

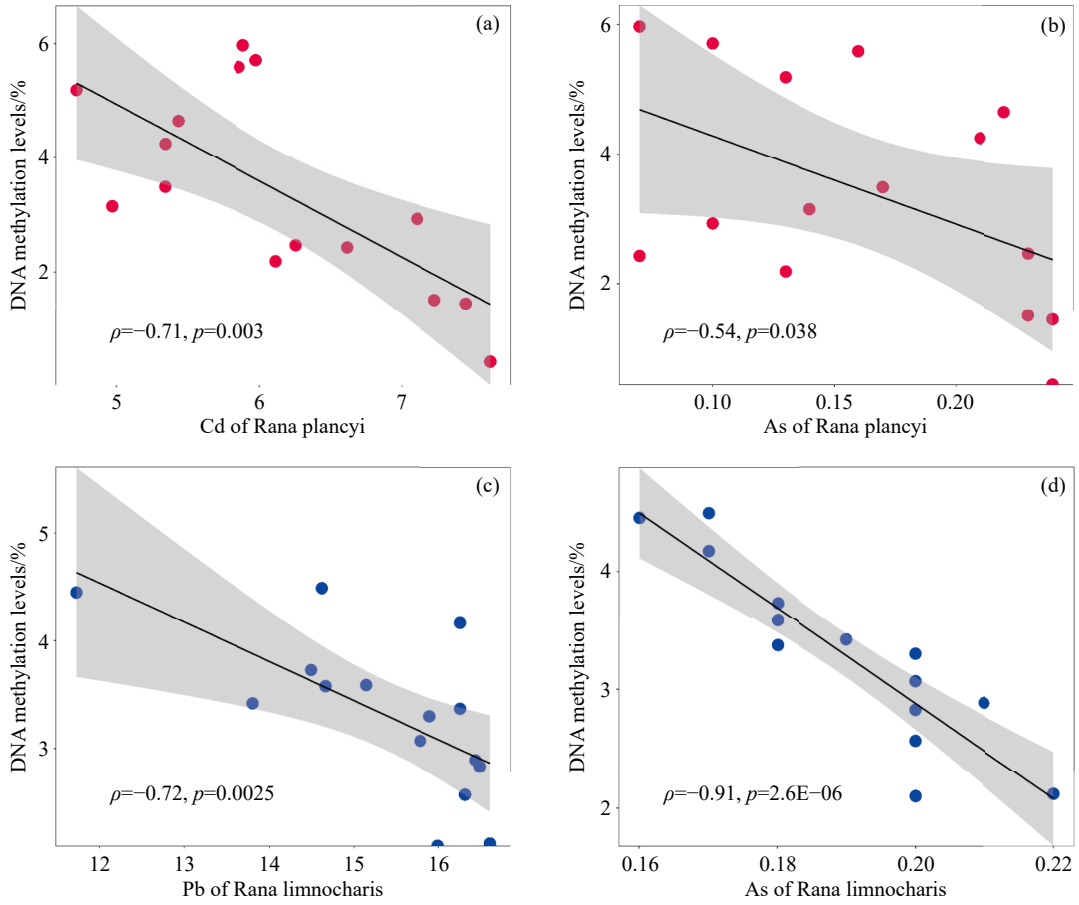

Fig. 6. Spearman correlation coefficient between trace metals and DNA methylation in frog tissues.

contamination across interconnected environmental compartments. River systems exhibited downstream Cd/Pb enrichment exceeding WHO guidelines by 11–15×, while agricultural soils showed extreme Cd contamination (15× background levels) with Igeo indices confirming moderate-to-strong anthropogenic loading. Atmospheric particulates demonstrated Pb/Cr dominance from smelting emissions, with lichen biomonitoring revealing 100–1000× baseline exceedances.

(ii) Cd/Pb exhibited exceptional biotransfer efficiency, evidenced by BCF>1000 in amphibians and BAF>2.5 in earthworms. Genome-wide DNA hypomethylation in biota (2.4%–6.6% reduction vs. controls) established dose-dependent relationships with Cd/Pb/As exposure (ρ=−0.56 to −0.91), implicating metal-induced epigenetic dysregulation as a novel toxicity pathway in mining ecosystems.

(iii) Ecological risk indices identified Cd as the dominant stressor, contributing >80% of total risk (Eri=554.25 in water; RI⩾300 in soil). Human health modeling revealed atmospheric Cr-driven carcinogenic risks (TCR=4.11×10^{-5} for adults), exceeding acceptable thresholds despite low absolute concentrations, highlighting bioavailability-mediated risk amplification.

(iv) The developed source-media-biota-risk framework advances mining pollution assessment by: quantifying cross-media transfer coefficients (e.g., Cd BCF=892–1096), establishing DNA methylation as sensitive epigenetic biomarker, demonstrating adult susceptibility reversal in risk paradigms.

CRediT authorship contribution statement

Xiao-tao Zhang conceptualized the entire paper and prepared the manuscript. Man-dan Huang participated in the drawing illustrations and preparation of manuscript. Bin Shen and Zhi-hang Xin participated in the conception and article verification. Shan-hong Lan and Jun-jie Hu supervised the field investigation and sample collection of the whole project.

Declaration of competing interest

The authors declare no conflict to interest.

Acknowledgments

The present work was financially supported by the Fundation of Key Laboratory of Ministry of Natural Resources for Eco-geochemistry (ZSDHJJ202202), and Geological Investigation and Evaluation of Shale Gas in Complex Structural Areas of the Middle Yangtze plate (DD20250200604) of China Geological Survey, the Natural Science Foundation of Guangdong Province, China (2023A1515140061), and the Dongguan Science and Technology of Social Development Program (20231800935842, 20231800940562).

Appendix A. Supplementary data

Supplementary data (Table S1-S13) to this article can be found online at doi: 10.31035/cg20250074.

References

Adhikari S, Jordaan A, Beukes JP, Siebert SJ. 2022. Anthropogenic sources dominate foliar chromium dust deposition in a mining-based urban region of south Africa. International Journal of Environmental Research and Public Health, 19(4), 2072. doi: 10.3390/ijerph19042072.

Bai HL, Liu GN, Chen DL, Xing ZS, Wang YH, Wang J, Zhao YY. 2024. Heavy metal pollution in sediments of the Yu River in a polymetallic ore concentration area: temporal–spatial variation, risk assessment, and sources apportionment. Sustainability, 16(3), 1154. doi: 10.3390/su16031154.

Bashkin VN. 2007. Modern biogeochemistry: Environmental Risk Assessment. Springer Dordrecht, 215-228.

Belle GN, Schoeman Y, Oberholster PJ. 2024. Source to receptor: assessing health risks from heavy metal exposure in mining soils. Minerals, 14(9), 858. doi: 10.3390/min14090858.

Bing HJ, Wu YH, Li J, Xiang ZX, Luo XS, Zhou J, Sun HY, Zhang G. 2019. Biomonitoring trace element contamination impacted by atmospheric deposition in China's remote mountains. Atmospheric Research, 224, 30–41. doi: 10.1016/j.atmosres.2019.03.018.

Cai K, Li C. 2022. Ecological risk, input flux, and source of heavy metals in the agricultural plain of Hebei Province, China. International Journal of Environmental Research and Public Health, 19(4), 2288. doi: 10.3390/ijerph19042288.

Chen XH, Yu B, Wang XD, Zhu RR, Zhang LF. 2025. The uptake and in-vivo migration of Hg by plants: a critical review. Reviews in Environmental Science and Bio/Technology, 24(1), 145–165. doi: 10.1007/s11157-024-09714-2.

Chen YZ, Ning YQ, Bi XY, Liu JL, Yang SC, Liu ZF, Huang WM. 2022. Pine needles as urban atmospheric pollution indicators: heavy metal concentrations and Pb isotopic source identification. Chemosphere, 296, 134043. doi: 10.1016/j.chemosphere.2022.134043.

Chi WT, Yang Y, Zhang K, Wang P, Du YH, Li XM, Sun Y, Liu TX, Li FB. 2022. Seawater intrusion induced cadmium activation via altering its distribution and transformation in paddy soil. Chemosphere, 307, 135805. doi: 10.1016/j.chemosphere.2022.135805.

Chien C, Benaltabet T, Torfstein A, Paytan A. 2019. Contributions of atmospheric deposition to Pb concentration and isotopic composition in seawater and particulate matters in the gulf of Aqaba, Red Sea. Environmental Science & Technology, 53(11), 6162–6170. doi: 10.1021/acs.est.9b00505.

Chris DI, Onyena AP, Sam K. 2023. Evaluation of human health and ecological risk of heavy metals in water, sediment and shellfishes in typical artisanal oil mining areas of Nigeria. Environmental Science and Pollution Research, 30(33), 80055–80069. doi: 10.1007/s11356-023-27932-z.

Demková L, Jezný T, Bobuľská L. 2017. Assessment of soil heavy metal pollution in a former mining area - before and after the end of mining activities. Soil and Water Research, 12(4), 229–236. doi: 10.17221/107/2016-SWR.

Ediagbonya TF, Ogunjobi JA, Odinaka CV, Adenikinju CA. 2022. Bioaccumulation of elemental concentrations in sediment and frog (Pyxicephalus edulis) in Igbeebo River, Ondo State, Nigeria. Chemistry Africa, 5(4), 1153–1165. doi: 10.1007/s42250-022-00406-4.

Edo GI, Samuel PO, Oloni GO, Ezekiel GO, Ikpekoro VO, Obasohan P, Ongulu J, Otunuya CF, Opiti AR, Ajakaye RS, Essaghah AEA, Agbo JJ. 2024. Environmental persistence, bioaccumulation, and ecotoxicology of heavy metals. Chemistry and Ecology, 40(3), 322–349. doi: 10.1080/02757540.2024.2306839.

Ersoz M, Barrott L. 2012. Best Practice Guide on Metals Removal from Drinking Water by Treatment, Metals and Related Substances in Drinking Water Series. IWA Publishing, 245–279.

Faraji M, Alizadeh I, Oliveri Conti G, Mohammadi A. 2023. Investigation of health and ecological risk attributed to the soil heavy metals in Iran: systematic review and meta-analysis. Science of the Total Environment, 857, 158925. doi: 10.1016/j.scitotenv.2022.158925.

Galati S, Gullì M, Giannelli G, Furini A, DalCorso G, Fragni R, Buschini A, Visioli G. 2021. Heavy metals modulate DNA compaction and methylation at CpG sites in the metal hyperaccumulator Arabidopsis halleri. Environmental and Molecular Mutagenesis, 62(2), 133–142. doi: 10.1002/em.22421.

Gantayat RR, Elumalai V. 2024. Salinity-induced changes in heavy metal behavior and mobility in semi-arid coastal aquifers: a comprehensive review. Water, 16(7), 1052. doi: 10.3390/w16071052.

Garty J. 2001. Biomonitoring atmospheric heavy metals with lichens: Ttheory and application. Critical Reviews in Plant Sciences, 20(4), 309–371. doi: 10.1080/20013591099254.

Gasparatos D, Barbayiannis N. 2018. The origin of nickel in soils. Nickel in Soils and Plants. Boca Raton: CRC Press, 105–128. doi: 10.1201/9781315154664-5.

Goodfellow BW, Hilley GE, Webb SM, Sklar LS, Moon S, Olson CA. 2016. The chemical, mechanical, and hydrological evolution of weathering granitoid. Journal of Geophysical Research: Earth Surface, 121(8), 1410–1435. doi: 10.1002/2016JF003822.

Gruss I, Lallaouna R, Twardowski J, Magiera-Dulewicz J, Twardowska K. 2024. Collembola growth in heavy metal-contaminated soils. Scientific Reports, 14(1), 27998. doi: 10.1038/s41598-024-79766-5.

Harmens H, Ilyin I, Mills G, Aboal JR, Alber R, Blum O, Coşkun M, De Temmerman L, Fernández JÁ, Figueira R, Frontasyeva M, Godzik B, Goltsova N, Jeran Z, Korzekwa S, Kubin E, Kvietkus K, Leblond S, Liiv S, Magnússon SH, Maňkovská B, Nikodemus O, Pesch R, Poikolainen J, Radnović D, Rühling Å, Santamaria JM, Schröder W, Spiric Z, Stafilov T, Steinnes E, Suchara I, Tabors G, Thöni L, Turcsányi G, Yurukova L, Zechmeister HG. 2012. Country-specific correlations across Europe between modelled atmospheric cadmium and lead deposition and concentrations in mosses. Environmental Pollution, 166, 1–9. doi: 10.1016/j.envpol.2012.02.013.

Heller-Zeisler S, Zeisler R, Zeiller E, Parr RM, Radecki Z, Burns KI, De Regge P. 1999. Report on the intercomparison run for the determination of trace and minor elements in lichen material IAEA-336. NAHRES-33, (IAEA/AL/79). International Atomic Energy Agency, Vienna.

Hossain MB, Vahter M, Concha G, Broberg K. 2012. Low-level environmental cadmium exposure is associated with DNA hypomethylation in Argentinean women. Environmental Health Perspectives, 120(6), 879–884. doi: 10.1289/ehp.1104600.

Howlader M, Mamun AM, Rahman MM, Rahman MH, Chandra Swarnokar S, Sultana M, Rahman MT, Das TK. 2025. Spatial characteristics and health risks assessments of trace metal pollution from road dusts in the industrialized city of Bangladesh. Heliyon, 11(2), e42008. doi: 10.1016/j.heliyon.2025.e42008.

Hu JJ, Liu JH, Li JY, Lv XM, Yu LL, Wu KM, Yang Y. 2021. Metal contamination, bioaccumulation, ROS generation, and epigenotoxicity influences on zebrafish exposed to river water polluted by mining activities. Journal of Hazardous Materials, 405, 124150. doi: 10.1016/j.jhazmat.2020.124150.

Jahandari A, Abbasnejad B. 2024. Environmental pollution status and

health risk assessment of selective heavy metal(oid)s in Iran's agricultural soils: a review. Journal of Geochemical Exploration, 256, 107330. doi: 10.1016/j.gexplo.2023.107330.

Jia XY, Jiang L, Xia TX, Zhong MS, Zhang LN, Wang JF, Liu H. 2012. Comparison of RBCA, CLEA and CalTOX for health risk assessment of a Benzo[a]pyrene contaminated site. Asian Journal of Ecotoxicology, 7(3), 277–284 (in Chinese with English abstract).

Jing MY, Zhang HC, Wei MY, Tang YW, Xia Y, Chen YH, Shen ZG, Chen C. 2022. Reactive oxygen species partly mediate DNA methylation in responses to different heavy metals in Pokeweed. Frontiers in Plant Science, 13, 845108. doi: 10.3389/fpls.2022.845108.

Köse E. 2024. The bioaccumulation of heavy metals in the water and tissues of invasive fish Carassius gibelio (Bloch, 1782) and non-carcinogenic health risk assessment from Meriç Delta wetland, Türkiye. Biological Trace Element Research, . doi: 10.1007/s12011-024-04367-2.

Kumari M, Bhattacharya T. 2023. A review on bioaccessibility and the associated health risks due to heavy metal pollution in coal mines: content and trend analysis. Environmental Development, 46, 100859. doi: 10.1016/j.envdev.2023.100859.

Laidlaw MAS, Mielke HW, Filippelli GM. 2023. Assessing unequal airborne exposure to lead associated with race in the USA. GeoHealth, 7(7), e2023GH000829. doi: 10.1029/2023GH000829.

Liu HL, Wang HT, Zhao H, Wang H, Xia RZ, Wang XZ, Li M, Zhou J. 2024. Speciation, bioaccumulation, and toxicity of the newly deposited atmospheric heavy metals in soil-earthworm (Eisenia fetida) system near a large copper smelter. Science of the Total Environment, 924, 171700. doi: 10.1016/j.scitotenv.2024.171700.

Liu HL, Zhou Jun, Li M, Obrist D, Wang XZ, Zhou J. 2021. Chemical speciation of trace metals in atmospheric deposition and impacts on soil geochemistry and vegetable bioaccumulation near a large copper smelter in China. Journal of Hazardous Materials, 413, 125346. doi: 10.1016/j.jhazmat.2021.125346.

Mao SX, Zhao QC, Ma SY, Du YB, Shi JS, Zou JC, Qiu ZL, Yu CH. 2024. Heavy metal pollution pressure in gold mines shows overall suppressed biochemical sulfur cycle. International Biodeterioration & Biodegradation, 191, 105807. doi: 10.1016/j.ibiod.2024.105807.

Marrugo-Negrete J, Pinedo-Hernández J, Marrugo-Madrid S, Díez S. 2021. Assessment of trace element pollution and ecological risks in a river basin impacted by mining in Colombia. Environmental Science and Pollution Research, 28(1), 201–210. doi: 10.1007/s11356-020-10356-4.

Matlock M, Morgan R, White K, Avery R. 2005. An environmental risk assessment using CalTOX. WIT Transactions on Ecology and the Environment, 85.

Moaref S, Sekhavatjou MS, Hosseini Alhashemi A. 2014. Determination of trace elements concentration in wet and dry atmospheric deposition and surface soil in the largest industrial city, Southwest of Iran. International Journal of Environmental Research, 8(2). doi: 10.22059/ijer.2014.724.

Moldovan A, Török AI, Kovacs E, Cadar O, Mirea IC, Micle V. 2022. Metal contents and pollution indices assessment of surface water, soil, and sediment from the arieş river basin mining area, Romania. Sustainability, 14(13), 8024. doi: 10.3390/su14138024.

Ni SQ, Liu GN, Zhao YY, Zhang CQ, Wang AY. 2023. Distribution and source apportionment of heavy metals in soil around Dexing copper mine in Jiangxi Province, China. Sustainability, 15(2), 1143. doi: 10.3390/su15021143.

Nohara K, Baba T, Murai H, Kobayashi Y, Suzuki T, Tateishi Y, Matsumoto M, Nishimura N, Sano T. 2011. Global DNA methylation in the mouse liver is affected by methyl deficiency and arsenic in a sex-dependent manner. Archives of Toxicology, 85(6), 653–661. doi: 10.1007/s00204-010-0611-z.

Pal D, Tripathi A, Hussain T, Jindal T, Shukla K. 2022. Assessment of impact of human interferences including mining activities on water quality of Banas River, Rajsamand City, India. Asian Journal of Chemistry, 34(12), 3299–3307. doi: 10.14233/ajchem.2022.24032.

Paoli L, Pisani T, Guttová A, Sardella G, Loppi S. 2011. Physiological and chemical response of lichens transplanted in and around an industrial area of south Italy: relationship with the lichen diversity. Ecotoxicology and Environmental Safety, 74(4), 650–657. doi: 10.1016/j.ecoenv.2010.10.011.

Park S, Kim Y. 2016. Mineralogical changes and distribution of heavy metals caused by the weathering of hydrothermally altered, pyrite-rich andesite. Environmental Earth Sciences, 75(15), 1125. doi: 10.1007/s12665-016-5915-8.

Priyadarshani S, Madhushani WAN, Jayawardena UA, Wickramasinghe DD, Udagama PV. 2015. Heavy metal mediated immunomodulation of the Indian green frog, Euphlyctis hexadactylus (Anura: Ranidae) in urban wetlands. Ecotoxicology and Environmental Safety, 116, 40–49. doi: 10.1016/j.ecoenv.2015.02.037.

Ren Z, Leng CB, Yang YP, Chen JJ, Wang AD, Wang SL. 2025. Microstructure and trace element occurrence in molybdenite (MoS_2) from the Dexing ore field: Implications for the differential enrichment of rhenium. Ore Geology Reviews, 177, 106473. doi: 10.1016/j.oregeorev.2025.106473.

Robaldi-Vázquez MP, López-Acosta NP, Ceniceros-Gómez AE, Barba-Galdámez DF. 2025. A method to analyze field predictors of heavy metal pollution in riparian soils and plants. Ecological Indicators, 173, 113323. doi: 10.1016/j.ecolind.2025.113323.

Rudnicka-Kępa P, Bełdowska M, Zaborska A. 2024. Enhanced heavy metal discharges to marine deposits in glacial bays of two Arctic fjords (Hornsund and Kongsfjorden). Journal of Marine Systems, 241, 103915. doi: 10.1016/j.jmarsys.2023.103915.

Safe YL, Palenzona M, Lucchi LD, Domini CE, Pereyra MT. 2023. Multi-year monitoring of atmospheric dust fall as a sink for lead in an agro-industrial and petrochemical city of Argentina. Environmental Geochemistry and Health, 45(7), 4817–4835. doi: 10.1007/s10653-023-01539-2.

Santos NL, Klammler HR, Leal LRB. 2022. Modeling urban atmospheric lead dispersion from a mining tailings basin in Bahia, Brazil. Anuário do Instituto de Geociências, 45. doi: 10.11137/1982-3908_2022_45_48909.

Setu S, Strezov V. 2025. Impacts of non-ferrous metal mining on soil heavy metal pollution and risk assessment. Science of The Total Environment, 969, 178962. doi: 10.1016/j.scitotenv.2025.178962.

Shafiq S, Ali A, Sajjad Y, Zeb Q, Shahzad M, Khan AR, Nazir R, Widemann E. 2020. The interplay between toxic and essential metals for their uptake and translocation is likely governed by DNA methylation and histone deacetylation in maize. International Journal of Molecular Sciences, 21(18), 6959. doi: 10.3390/ijms21186959.

Shafiq S, Zeb Q, Ali A, Sajjad Y, Nazir R, Widemann E, Liu LY. 2019. Lead, cadmium and zinc phytotoxicity alter DNA methylation levels to confer heavy metal tolerance in wheat. International Journal of Molecular Sciences, 20(19), 4676. doi: 10.3390/ijms20194676.

Simatupang CA, Santhaweesuk K, Pongkiatkul P, Strezov V, Boontanon N, Jindal R, Boontanon SK. 2025. Source identification using principal component analysis and health risk assessment of heavy metals contamination in PM2. 5 near an industrial area in Thailand. Exposure and Health, 17(1), 245–264. doi: 10.1007/s12403-024-00657-1.

Singh D, Bist P, Choudhary S. 2025. Effect of co-exposure to multiple metals (Pb, Cd, Cr, Hg, Fe, Mn and Ni) and metalloid (As) on liver function in Swiss albino mice. BioMetals, 38(1), 135–152. doi: 10.1007/s10534-024-00643-9.

Singh SM, Sharma J, Gawas-Sakhalkar P, Upadhyay AK, Naik S, Pedneker SM, Ravindra R. 2013. Atmospheric deposition studies of

heavy metals in Arctic by comparative analysis of lichens and cryoconite. Environmental Monitoring and Assessment, 185(2), 1367–1376. doi: 10.1007/s10661-012-2638-5.

Søndergaard J, Bach L, Asmund G. 2013. Modelling atmospheric bulk deposition of Pb, Zn and Cd near a former Pb–Zn mine in West Greenland using transplanted Flavocetraria nivalis lichens. Chemosphere, 90(10), 2549–2556. doi: 10.1016/j.chemosphere.2012.10.097.

Swartjes FA. 1999. Risk‐based assessment of soil and groundwater quality in the Netherlands: standards and remediation urgency. Risk Analysis, 19(6), 1235–1249. doi: 10.1023/A:1007003332488.

Tabassum S, Kotnala CB, Salman M, Tariq M, Khan AH, Khan NA. 2024. The impact of heavy metal concentrations on aquatic insect populations in the Asan Wetland of Dehradun, Uttarakhand. Scientific Reports, 14(1), 4824. doi: 10.1038/s41598-024-52522-5.

Tariq A, Farhat F. 2025. Insights into microbe assisted remediation in plants: a brief account on mechanisms and multi-omic strategies against heavy metal toxicity. Stress Biology, 5(1), 4. doi: 10.1007/s44154-024-00168-8.

Tatlı H, Gedik K, Altunışık A. 2024. Investigation of heavy metals in tissues and habitats of three edible frogs from Türkiye. Environmental Science and Pollution Research, 31(5), 7806–7817. doi: 10.1007/s11356-023-31226-9.

Tran TS, Dinh VC, Nguyen TAH, Kim KW. 2022. Soil contamination and health risk assessment from heavy metals exposure near mining area in Bac Kan province, Vietnam. Environmental Geochemistry and Health, 44(4), 1189–1202. doi: 10.1007/s10653-021-01168-7.

USEPA. 2001. Risk assessment guidance for superfund: volume III — part a, process for conducting probabilistic risk assessment. US environmental protection agency, Washington, DC.

Wang K, Qiao YH, Zhang HQ, Yue SZ, Li HF, Ji XH, Liu LS. 2018. Bioaccumulation of heavy metals in earthworms from field contaminated soil in a subtropical area of China. Ecotoxicology and Environmental Safety, 148, 876–883. doi: 10.1016/j.ecoenv.2017.11.058.

World Health Organization. 2017. Guidelines for drinking-water quality: fourth edition incorporating first addendum, 4th ed. , 1st add. ed. World Health Organization, Geneva.

Wu XH, Ouyang Y, Wang B, Lin J, Bai Y. 2020. Hypermethylation of the IRAK3-Activated MAPK signaling pathway to promote the development of glioma. Cancer Management and Research, 12, 7043–7059. doi: 10.2147/CMAR.S252772.

Zheng LL, Zhou ZK, Rao MM, Sun ZX. 2020. Assessment of heavy metals and arsenic pollution in surface sediments from rivers around a uranium mining area in east China. Environmental Geochemistry and Health, 42(5), 1401–1413. doi: 10.1007/s10653-019-00428-x.

Zhou Q, Jiang YH, Liao SY, Zhao P, Jia RY, Liu Z, Wang GC, Ni CY. 2016. Pertrogenesis and tectonic implications of the late Jurassic basic rocks from the northern Shi-Hang zone, southeast China. Island Arc, 25(3), 235–250. doi: 10.1111/iar.12147.

Zhu Y, An YF, Li XY, Cheng L, Lv SJ. 2024. Geochemical characteristics and health risks of heavy metals in agricultural soils and crops from a coal mining area in Anhui province, China. Environmental Research, 241, 117670. doi: 10.1016/j.envres.2023.117670.